PHYSICAL REVIEW C **88**, 025502 (2013)

Relativistic description of final-state interactions in neutral-current neutrino and antineutrino cross sections

R. González-Jiménez and J. A. Caballero
Departamento de Física Atómica, Molecular y Nuclear, Universidad de Sevilla, 41080 Sevilla, Spain

Andrea Meucci and Carlotta Giusti
Dipartimento di Fisica, Università degli Studi di Pavia, and INFN, Sezione di Pavia, Via A. Bassi 6, I-27100 Pavia, Italy

M. B. Barbaro
Dipartimento di Fisica, Università di Torino and INFN, Sezione di Torino, Via P. Giuria 1, 10125 Torino, Italy

M. V. Ivanov
Grupo de Física Nuclear, Departamento de Física Atómica, Molecular y Nuclear, Universidad Complutense de Madrid, CEI Moncloa, 28040 Madrid, Spain and Institute for Nuclear Research and Nuclear Energy, Bulgarian Academy of Sciences, Sofia 1784, Bulgaria

J. M. Udías
Grupo de Física Nuclear, Departamento de Física Atómica, Molecular y Nuclear, Universidad Complutense de Madrid, CEI Moncloa, 28040 Madrid, Spain

(Received 10 July 2013; published 21 August 2013)

We evaluate semi-inclusive neutral-current quasielastic differential neutrino and antineutrino cross sections within the framework of the relativistic impulse approximation. The results of the relativistic mean-field and of the relativistic Green's function models are compared. The sensitivity to the strange-quark content of the nucleon form factor is also discussed. The results of the models are compared with the MiniBooNE experimental data for neutrino scattering. Numerical predictions for flux-averaged antineutrino scattering cross sections are also presented.

DOI: 10.1103/PhysRevC.88.025502 PACS number(s): 25.30.Pt, 13.15.+g, 24.10.Jv

I. INTRODUCTION

The results on neutrino oscillations published by different collaborations [1–15] have raised a large debate over the properties of neutrinos that could lead to a more complete understanding of neutrino physics. Because of the interest in oscillation measurements, various experimental neutrino-nucleus differential cross sections have been presented [16–21] and are planned in the near future [22–24]. A clear understanding of neutrino-nucleus reactions with a precise determination of differential cross sections is crucial for a proper analysis of the experimental data.

The MiniBooNE Collaboration has recently reported [18] a measurement of the neutral-current elastic (NCE) flux-averaged differential neutrino cross section on CH_2 as a function of the four-momentum transferred squared, Q^2. The energy region considered in the MiniBooNE experiments, with average neutrino energy of $\approx$0.8 GeV, requires the use of a relativistic model with an adequate description of nuclear dynamics and current operators. The relativistic Fermi gas (RFG) model cannot reproduce the data unless calculations are performed with a value of the axial mass M_A significantly larger ($M_A = 1.39 \pm 0.11$ GeV/c^2) than the world average value from the deuterium data of $M_A \simeq 1.03$ GeV/c^2 [25,26]. It is reasonable to assume the larger axial mass required by the RFG as an effective value to incorporate into the calculations of nuclear effects which are not included in the RFG. A precise knowledge of lepton-nucleus cross sections, where uncertainties on nuclear effects are reduced as much as possible, is mandatory and a comparison between the results of different models can be helpful to disentangle different physics aspects involved in the scattering process.

It would be a sound strategy to require that any nuclear model used to describe neutrino-nucleus scattering succeed in the description of available electron scattering data in similar kinematic regions [27]. At intermediate energy, quasielastic (QE) electron scattering calculations [28,29], which are able to successfully describe a wide number of experimental data, can provide a useful tool to study neutrino-induced processes. However, some of these models based on the impulse approximation (IA) have been shown to be unable to describe the MiniBooNE data for both charged-current (CC) and neutral-current (NC) reactions [30–33]. This has been viewed as an indication that the reaction can have significant contributions from effects beyond the IA. The contribution of multinucleon excitations to neutrino-nucleus scattering [34–40] has been found sizable and able to bring the theory in agreement with the MiniBooNE cross sections without the need to increase the axial mass M_A. On the other hand, a relativistic calculation of two-particle–two-hole excitations, performed for both electron and neutrino scattering [41–44], has shown that two body currents give a more modest contribution at MiniBooNE kinematics and are unable to fully account for the data. Other models invoke an enhancement of the magnetic response rather than a modification on the axial mass to get agreement with the MiniBooNE data [45,46].

A deeper understanding of the reaction dynamics would require a careful evaluation of all nuclear effects and of the relevance of multinucleon emission and of some non-nucleonic contributions [47–51]. Previous studies have clearly stated the relevance of final-state interactions (FSI) to reproduce the exclusive $(e, e'p)$ cross section within the distorted-wave impulse approximation (DWIA) [28,29,52–57] and the use of a complex optical potential (OP). The imaginary part of the OP produces an absorption that reduces the cross section and accounts partly for the loss of the incident flux to the open inelastic channels. For the case of inclusive scattering, where only the emitted lepton is detected, all elastic and inelastic channels contribute, and a different treatment of FSI is required: since all final-state channels are retained, the flux lost in a channel is redistributed in the other channels, and in the sum over all the channels the total flux must be conserved.

FSI have been considered in relativistic calculations for the inclusive QE electron- and neutrino-nucleus scattering under different approaches [58–70]. The simplest one corresponds to the relativistic plane-wave impulse approximation (RPWIA), where FSI are neglected. In some DWIA calculations FSI effects are incorporated in the final nucleon state by using real potentials, either retaining only the real part of the relativistic energy-dependent complex optical potential (denoted as rROP) or using the same relativistic mean-field potential considered in describing the initial nucleon state (RMF) [58,71]. Note that the RMF, because of the use of the same strong energy-independent real potential for both bound and scattering states, fulfills the dispersion relation [72] and maintains the continuity equation.

A different description of FSI involves the use of relativistic Green's function (RGF) techniques [61,62,68,69,73–78]. In the RGF model the components of the nuclear response are written in terms of the single-particle optical model Green's function; its spectral representation, which is based on a biorthogonal expansion in terms of a non-Hermitian OP $\mathcal{H}$ and of its Hermitian conjugate $\mathcal{H}^\dagger$, can be exploited to avoid the explicit calculation of the single-particle Green's function and obtain the components of the hadron tensor [61,62]. Calculations require matrix elements of the same type as the DWIA ones of the exclusive $(e, e'p)$ process in [53] but involve eigenfunctions of both $\mathcal{H}$ and $\mathcal{H}^\dagger$, where the imaginary part has an opposite sign and gives in one case a loss and in the other case a gain of strength. The RGF formalism makes it possible to reconstruct the flux lost into nonelastic channels in the case of the inclusive response starting from the complex OP which describes elastic nucleon-nucleus scattering data. Moreover, a consistent treatment of FSI in both exclusive and inclusive scattering is provided, and, because of the analyticity properties of the OP, the Coulomb sum rule is fulfilled [62,72,73].

A comparison among these different descriptions of FSI has been presented in [68] for inclusive QE electron scattering, in [69] for charged-current quasielastic (CCQE) neutrino scattering, and in [79] with the CCQE MiniBooNE data. The behavior of electron scattering data and their related scaling and superscaling functions are successfully described by both RMF and RGF models. In the case of neutrinos, the shape of the experimental CCQE cross sections is well reproduced by both models, although the RMF generally underpredicts the CCQE MiniBooNE data, while the RGF can reproduce its magnitude for some particular choices of the relativistic potential without the need to increase the standard value of the axial mass.

In this work we extend the comparison between the results of the RGF and RMF models to NCE scattering. We note that the RGF is appropriate for an inclusive process where only the emitted lepton is detected, whereas in NCE scattering the final lepton is usually not detected and it is the nucleon in the final state that triggers the event detections. Thus NCE cross sections are usually semi-inclusive in the hadronic sector, where events for which at least one nucleon in the final state is detected are experimentally selected. The description of semi-inclusive NCE scattering with the RGF approach can recover important contributions that are not present in the RDWIA, for which the semi-inclusive cross section is obtained from the sum of all the integrated single-nucleon knockout channels plus the absorption produced in each channel by the imaginary part of the optical potential. This is appropriate for exclusive scattering, but it neglects some final-state channels which can contribute to the semi-inclusive reaction. The RGF, however, describes the inclusive process and, as such, may include channels which are not present in the semi-inclusive NCE measurements. From this point of view, the RDWIA can represent a lower limit and the RGF an upper limit to the semi-inclusive NCE cross sections. In comparison with the MiniBooNE NCE data, the RDWIA generally underpredicts the experimental cross section, while the RGF results are in reasonable agreement with the NCE data [80].

It is not easy to disentangle the role of specific contributions which may be neglected in the RDWIA or spuriously added in the RGF, in particular if we consider that both RDWIA and RGF calculations make use of phenomenological optical potentials, obtained through a fit of elastic proton-nucleus scattering data. In order to clarify the content of the enhancement of the RGF cross sections compared to those of the IA models, a careful evaluation of all nuclear effects and of the relevance of multinucleon emission and of some non-nucleonic contributions [48] is required. The comparison with the results of the RMF model, where only the purely nucleonic contribution is included, can be helpful for a deeper understanding of nuclear effects, particularly FSI, which may play a crucial role in the analysis of upcoming scattering data, and of their influence in studies of neutrino oscillations at intermediate to high energies.

II. RESULTS

In this section the numerical results of the RGF and RMF models are compared for NCE neutrino and antineutrino scattering on ^{12}C. As a first step, we have proved that RPWIA cross sections evaluated with two independent computer programs (developed by the Pavia and Madrid-Sevilla groups) are almost identical. This gives us enough confidence on the reliability of both calculations, and it agrees with previous results found in [68] for the inclusive QE electron scattering and in [69] for CCQE neutrino-nucleus scattering. Then the

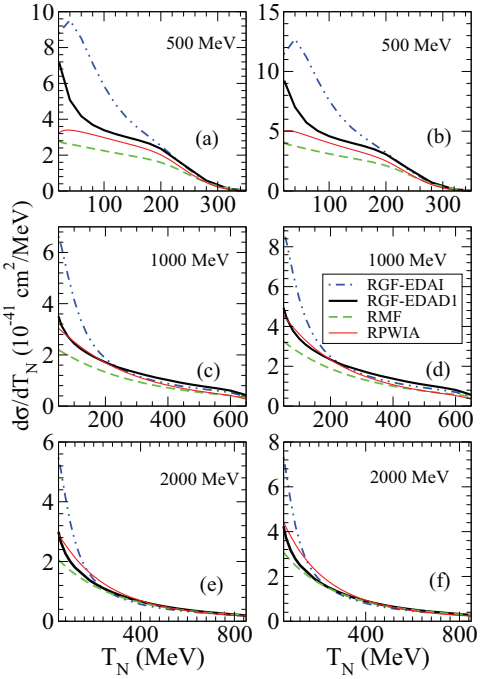

FIG. 1. (Color online) Differential cross sections of NCE neutrino scattering on ^{12}C as a function of the kinetic energy of the emitted proton [panels (a), (c), and (e)] or neutron [panels (b), (d), and (f)] at $\varepsilon_\nu = 500$, 1000, and 2000 MeV calculated in the RPWIA (thin solid lines), RMF (dashed lines), RGF-EDAD1 (thick solid lines), and RGF-EDAI (dash-dotted lines). The vector and axial-vector strange form factors have been fixed to zero.

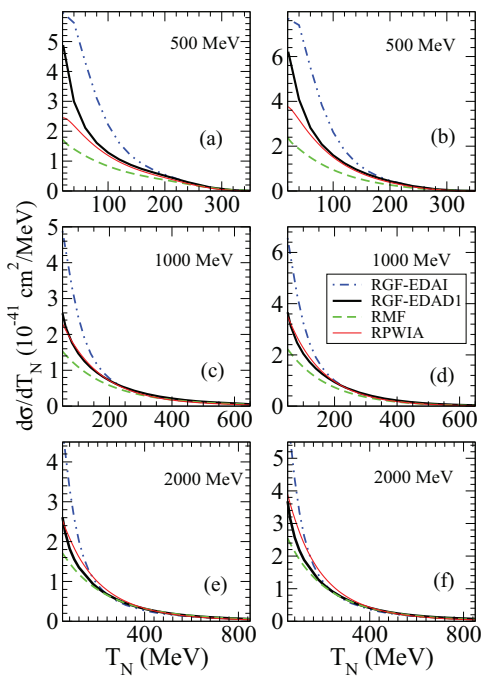

FIG. 2. (Color online) The same as in Fig. 1, but for antineutrino scattering.

comparison between the results corresponding to the RMF and RGF models is performed for the NCE neutrino- and antineutrino-induced cross sections and also for the ratio between proton- and neutron-knockout cross sections. In all the calculations presented in this work the bound nucleon states are taken as self-consistent Dirac-Hartree solutions derived within a relativistic mean-field approach using a Lagrangian containing σ, ω, and ρ mesons [81].

The differential cross sections of the NCE neutrino and antineutrino scattering, evaluated in the RPWIA, RMF, and RGF, are presented in Figs. 1 and 2 as a function of the kinetic energy of the emitted proton or neutron for three different (anti)neutrino energies $\varepsilon_{\nu(\bar{\nu})} = 500$, 1000, and 2000 MeV. The contribution from strange quarks to the vector and axial-vector form factors has been fixed to zero. In addition, we note that in all the calculations presented in this work we have used the standard value of the axial mass, $M_A = 1.03$ GeV. A different value of M_A would change the cross sections but not the comparison between the results of the different models. In the RGF calculations we have used two parametrizations for the relativistic OP of ^{12}C: the energy-dependent and A-dependent EDAD1 (where A is the atomic number) and the energy-dependent and A-independent EDAI phenomenological OPs of [82]. The EDAD1 parametrization is a global one, because it is obtained through a fit to elastic proton-scattering data on a wide range of nuclei and, as such, it depends on the atomic number A, whereas the EDAI OP is constructed only from elastic proton-^{12}C phenomenology [82]. It leads to a better description of the inclusive QE ^{12}C(e, e') experimental cross section, as well as to CCQE and NCE results that are in better agreement with the MiniBooNE data within the RGF approach [68,79,80,83].

The RMF gives cross sections that are generally 30% lower than the RPWIA ones at small outgoing nucleon kinetic energy T_N, but with a longer tail extending toward larger values of T_N, i.e., higher values of the transferred energy, that is attributable to the strong energy-independent scalar and vector potentials adopted in the RMF approach.

The RGF cross sections are generally larger than the RPWIA and the RMF ones. In the RGF the imaginary part of the optical potential redistributes the flux in all the final-state channels and, in each channel, the flux lost toward other channels is recovered by the flux gained from the other channels. The larger cross sections in the RGF arise from the translation to the strength of the overall effects of inelastic channels which are not included in the other models, such as, for instance, rescattering processes of the nucleon in its way out of the nucleus, non-nucleonic Δ excitations which may arise during nucleon propagation, or also some multinucleon processes. These contributions are not included explicitly in the RGF, but they all built phenomenologically on the absorptive imaginary part of the OP. Dispersion relations within the RGF would translate this strength into the inclusive RGF cross section. However, the RGF is appropriate for an inclusive process where only the emitted lepton is detected and can include contributions of channels which are present in an inclusive but not in a semi-inclusive reaction. From this point of view, the RGF can be considered as an upper limit to the NCE cross sections.

The comparison between the RGF results obtained with the EDAD1 and EDAI potentials can give an idea of how the predictions of the model are affected by uncertainties in the determination of the phenomenological OP. The differences depend on the energy and momentum transfer and are essentially attributable to the different imaginary part of the two potentials, which accounts for the overall effects of inelastic channels and is not univocally determined only from elastic phenomenology. In contrast, the real term is similar for different parametrizations and gives similar results.

The NCE experiments can also be used to look for possible strange-quark contributions in the nucleon. The role of strangeness contribution to the electric and magnetic nucleon form factors has been recently analyzed for parity-violating elastic electron scattering [84]. Specific values for the electric and magnetic strangeness were provided making use of all available data at different transferred momenta Q^2. The analysis of 1σ and 2σ confidence ellipses showed that zero electric and magnetic strangeness were excluded by most of the fits. However, the values of the strangeness in the electric and magnetic sectors compatible with the previous study lead to very minor effects in the separate proton and neutron contributions to the cross section for neutrino and antineutrino scattering. Moreover, these "small" effects tend to cancel, being negligible for the total differential cross sections. Although this cancellation also works for the axial-vector strangeness, its relative contribution to the separate proton and neutron cross sections is much larger than the one associated with the electric and magnetic channels. Therefore, in this paper we restrict ourselves to the influence of the axial-vector strangeness and consider how the NCE antineutrino cross sections change when the description of the axial-vector form factor of the nucleon is modified. It is a common prescription to apply the dipole parametrization to the strange axial form factor and to use the same value of the axial mass used for the nonstrange form factor as a cutoff; the strange axial coupling constant at $Q^2 = 0$ is Δs. A measurement of $\nu(\bar{\nu})$-proton elastic scattering at the Brookhaven National Laboratory at low Q^2 suggested a nonzero value for Δs [16,85]. The MiniBooNE Collaboration used the ratio of proton-to-nucleon NCE cross sections to extract $\Delta s = 0.08 \pm 0.26$ [18] based on the RFG with $M_A = 1.35\ \mathrm{GeV}/c^2$. The analysis performed in [86] with the RMF model led to $\Delta s = 0.04 \pm 0.28$, while the COMPASS Collaboration reported a negative $\Delta s = -0.08 \pm 0.01(\mathrm{stat.}) \pm 0.02(\mathrm{syst.})$ as a result of a measurement of the deuteron spin asymmetry [87], in agreement with the HERMES results [88].

The (anti)neutrino cross section can be understood essentially by analyzing the behavior of the longitudinal response L, the pure vector transverse response T, and the axial-vector transverse response T'. In Fig. 3 the relative importance of these three contributions to the NCE antineutrino differential cross section is presented for $\varepsilon_{\bar{\nu}} = 500$ MeV. For neutrino scattering the same separation holds but the T' response has opposite sign. The influence of Δs on each response, L, T, and T', and on separate proton and neutron events, is also explored. In order to avoid complications related to the description of the FSI and/or to uncertainties due to the particular model, calculations have been performed in the RPWIA. In the case

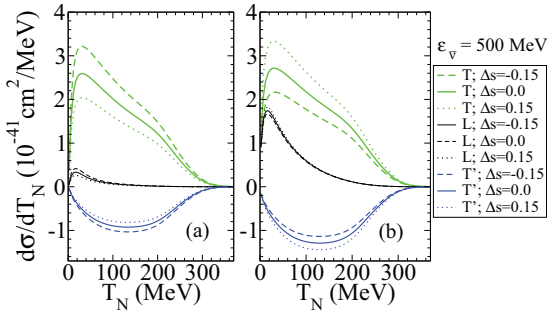

FIG. 3. (Color online) Separated longitudinal, L (central set of lines), transverse (symmetric), T (top set of lines), and transverse axial-vector (antisymmetric) T' (bottom set of lines) for the NCE antineutrino cross section at $\varepsilon_{\bar{\nu}} = 500$ MeV as a function of the emitted proton (a) or neutron (b) kinetic energy. Calculations are performed in the RPWIA. Solid, dashed, and dotted lines are the results with $\Delta s = 0.0$, -0.15, and $+0.15$, respectively.

of proton knockout, the transverse response T is larger by a factor of ≈ 2 than the transverse axial-vector response T', and the longitudinal response L is very small. In the case of neutron knockout, the T response is still larger than the T' one but the L contribution is significant. Note that the longitudinal response is to a large extent insensitive to strangeness.

The NCE differential cross sections are displayed in Fig. 4. The proton cross section decreases when increasing Δs, while the neutron cross section has the opposite behavior. Thus, the total proton+neutron cross section is almost independent of Δs in the range -0.15 to 0.15. This result is obtained for both neutrino and antineutrino scattering and is rather independent of the incident (anti)neutrino energy.

Determining the strangeness contribution to the axial form factor from measurements of NCE cross sections is not easy. Theoretical uncertainties on the approximations and on the ingredients of the models are usually larger than the uncertainty related to the strangeness content of the nucleon. From the experimental point of view, precise cross section measurements are not easy to make due to difficulties in the determination of the neutrino flux related to the nuclear model dependence. Therefore, ratios of cross sections have

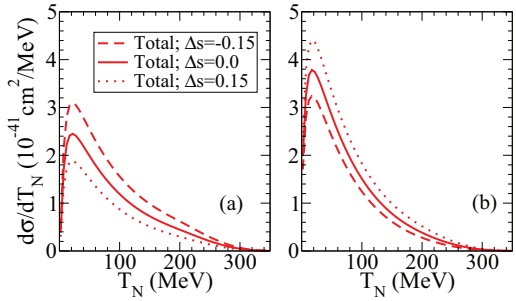

FIG. 4. (Color online) NCE antineutrino cross section at $\varepsilon_{\bar{\nu}} = 500$ MeV as a function of the emitted proton (a) or neutron (b) kinetic energy. Calculations are performed in the RPWIA. Solid, dashed, and dotted lines are the results with $\Delta s = 0.0$, -0.15, and $+0.15$, respectively.

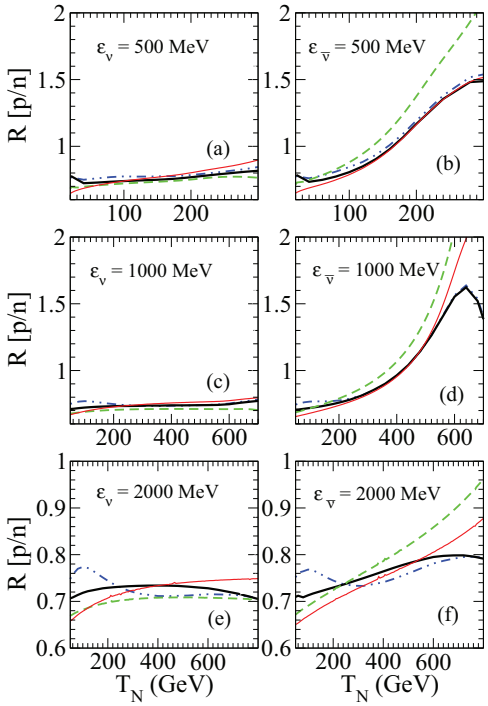

FIG. 5. (Color online) Ratio of proton-to-neutron cross sections as a function of the kinetic energy of the emitted nucleon for neutrino [panels (a), (c), and (e)] and antineutrino [panels (b), (d), and (f)]. Results of different descriptions of FSI are compared. Line conventions are as in Fig. 1. All the results are obtained with $\Delta s = 0$.

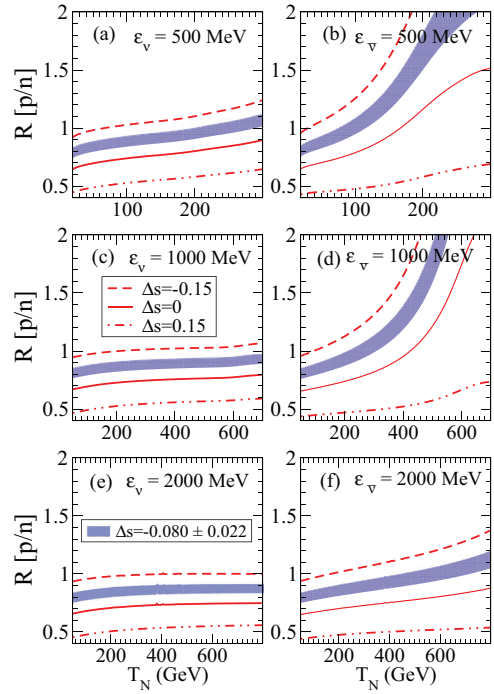

FIG. 6. (Color online) Ratio of proton-to-neutron cross sections as a function of the kinetic energy of the emitted nucleon for neutrino [panels (a), (c), and (e)] and antineutrino [panels (b), (d), and (f)]. Calculations are performed in the RPWIA and with different values of Δs. The shadowed band refers to results corresponding to the COMPASS-HERMES measurement for the axial strangeness.

been proposed as alternative and useful tools to search for strangeness effects. The ratio of proton-to-neutron cross sections was proposed and discussed in [89–95]. This ratio is very sensitive to strange-quark effects because the axial strangeness Δs interferes with the isovector contribution to the axial form factor $g_A \approx 1.27$ with one sign in the numerator and with the opposite sign in the denominator. In Fig. 5 we display our results for the p/n ratio for three different neutrino and antineutrino energies. In the case of ratios of cross sections the distortion effects are largely reduced and different models to describe FSI are expected to produce similar results. To make easier the comparison between neutrinos and antineutrinos we have chosen the same scale in both cases. This allows us to visualize clearly the different effects introduced by the models in both scattering reactions. In the case of neutrino scattering the p/n ratio is almost constant and the RPWIA, RMF, and RGF results coincide up to a few percent. As observed, in the region of small nucleon kinetic energy the main difference in the neutrino case comes from the RGF-EDAI model with a small bump (for $\varepsilon_\nu = 1$ and 2 GeV) that is not present in the other approaches. For larger T_N the ratio stabilizes, with the discrepancy among the different models being at most of the order of ∼4%–5%. Finally, the differences increase at the largest T_N values. Note that in this region the cross sections are very small and show a significant sensitivity to FSI and/or the thresholds used. The maximum uncertainty in the proton/neutron ratio linked to the different models is of the order of ∼15% ($\varepsilon_\nu = 500$ MeV) and ∼8% ($\varepsilon_\nu = 1$ and 2 GeV).

Larger differences are obtained in the case of antineutrino scattering, in particular for the RMF model, whose results are significantly enhanced with respect to the RGF ones for large values of T_N. Contrary to the case of neutrinos, where the ratio changes very smoothly with T_N, for antineutrinos the slope of the ratio goes up very fast with the nucleon energy. This reflects the different behavior shown by the proton and neutron cross sections against T_N. At intermediate nucleon energies the uncertainty among the various models is of the order of ∼12%–14%, with much larger discrepancies for increasing T_N values. However, in this energy region the cross section becomes significantly lower than its maximum and a very precise measurement is required to obtain a clear result. It is interesting to point out the similarity among the results corresponding to RGF-EDAI, RFG-EDAD1, and RPWIA at $\varepsilon_{\bar\nu} = 500$ and 1000 MeV.

In Fig. 6 the dependence of the RPWIA p/n ratio on the strange-quark contribution is presented. The ratio is enhanced when calculations are performed with a negative Δs and suppressed when a positive Δs is considered. In the case of antineutrino scattering the role of strangeness contribution is particularly significant when a negative Δs is assumed with a large peak at $T_N \approx 0.7\varepsilon_{\bar\nu}$. The sensitivity of the p/n ratio to Δs, as well as to the strange-quark contribution in the vector form factors, was analyzed in [65]. In particular, it was obtained that a moderately large and negative strangeness contribution to the magnetic moment of the nucleon can cancel the peak in the p/n ratio. Although a large strangeness

contribution to the vector form factors is not supported by any available experimental evidence [84], it would be anyhow intriguing to look for possible strangeness effects with a direct measurement of this quantity. We are aware that a precise measurement of the p/n ratio is a hard experimental task, but the first measurement of the MiniBooNE Collaboration [18] has proven the validity of this experimental technique and, hopefully, new data will be available in the future.

In the results of Fig. 6, the uncertainty in the proton/neutron ratio associated with the axial strangeness is quite large: in the case of neutrinos the ratio changes by a factor of 2 when going from positive ($\Delta s = 0.15$) to negative ($\Delta s = -0.15$) strangeness. This large range of variability of Δs is in accordance with $\nu(\bar{\nu})$ Brookhaven data [16,85] and also with the MiniBooNE results [18], but the COMPASS measurements suggest a narrower interval for the axial strangeness [87], which results in a reduced range of variation of the proton/neutron ratio. This is represented in Fig. 6 by the shadowed band that, as observed, is of the same order of magnitude as the uncertainties related to the distortion effects.

This sensitivity to Δs gets much larger for antineutrinos, where the ratio goes up very fast with increasing T_N values. However, as in the previous case for neutrinos, the range of variation in $R[p/n]$ associated to the COMPASS measurement is similar to the uncertainty introduced by nuclear model and/or distortion effects. Although this study is consistent with previous analyses, and it shows the capability of the ratio $R[p/n]$ as an useful observable in order to get precise information on the axial-vector strangeness content in the nucleon, the results in Fig. 6 indicate that, owing to the actual precision in the axial strangeness given by the COMPASS experiment, a deep and careful analysis of the uncertainties linked to ingredients of the calculation such as nuclear models or FSI is required.

III. RESULTS AT MINIBOONE KINEMATICS

The neutrino-nucleus NCE reaction at MiniBooNE can be considered as scattering of an incident neutrino or antineutrino with a single nucleon bound in carbon or free in hydrogen. Each contribution is weighted by an efficiency correction function and averaged over the experimental (anti)neutrino flux [96]. Different relativistic descriptions of FSI were presented and compared with the NCE MiniBooNE data in [80,86]. In Fig. 7 we present our RMF and RGF cross sections for NCE ($\nu N \to \nu N$) scattering and compare them with the experimental data, where the variable $Q^2_{QE} = 2m_N T$ is defined by assuming that the target nucleon is at rest, m_N being the nucleon mass and T the total kinetic energy of the outgoing nucleons. The RMF result has a too-soft Q^2 behavior to reproduce the experimental data at small Q^2, while the RGF produces larger cross sections, in better agreement with the data. The difference between the RGF results calculated with the two optical potentials is significant, particularly for small T_N (Q^2_{QE}) values. This is consistent with the large discrepancies shown by the cross sections evaluated at fixed neutrino and antineutrino energies (see Fig. 1). The RGF-EDAI cross section is in accordance with the shape and the magnitude

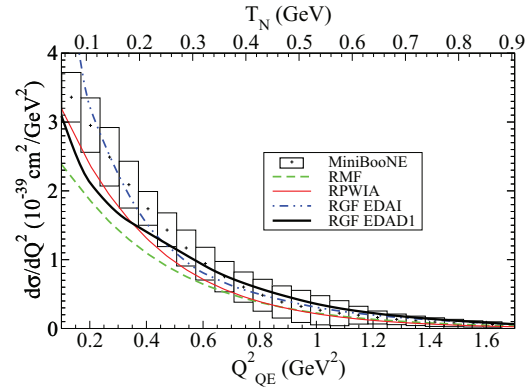

FIG. 7. (Color online) NCE flux-averaged ($\nu N \to \nu N$) cross section as a function of Q^2. Line conventions are as in Fig. 1. The data are from [18].

of the data. In contrast the RGF-EDAD1 result lies below the data at the smallest values of Q^2 considered in the figure. The RMF approach leads to the lowest cross section for low-to-intermediate values of the transferred four-momentum. Only for $Q^2_{QE} \geqslant 0.9$ GeV^2 is the RMF tail higher than the RPWIA result, but it still lies below the two RGF models. However, in this kinematical regime all the models are able to reproduce the data within the error bars.

The MiniBooNE Collaboration has collected also an extensive data set of neutral-current antineutrino events whose analysis is currently ongoing and some preliminaries results are available [97,98]. In Fig. 8 we show our predictions for the NCE MiniBooNE ($\bar{\nu}N \to \bar{\nu}N$) cross section. In these calculations we use the set of efficiency coefficients given in [18] for neutrino scattering. The selection for the antineutrino NCE sample is slightly different from the neutrino sample, and therefore the efficiencies are similar only as a first approximation, since they are expected to be a little bit different. However, even if it is not rigorous, the use of neutrino efficiencies for the antineutrinos is approximately correct. Similarly to the neutrino case, the RMF gives cross sections that are lower than the RPWIA ones whereas the RGF produces larger cross sections. This is consistent with the results shown in Fig. 2 for fixed antineutrino energies, where a significant

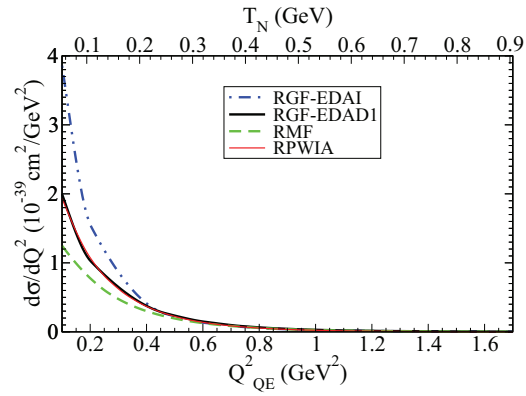

FIG. 8. (Color online) The same as in Fig. 7, but for the ($\bar{\nu}N \to \bar{\nu}N$) cross section.

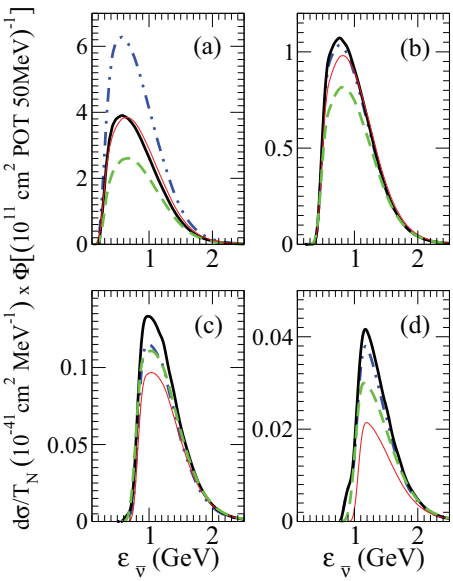

FIG. 9. (Color online) Product of the proton+neutron NCE antineutrino cross section and the antineutrino MiniBooNE flux [96] as a function of the antineutrino energy $\varepsilon_{\bar{\nu}}$ at four fixed values of the outgoing nucleon kinetic energy T_N: 108 (a), 252 (b), 540 (c), and 756 MeV (d). Line conventions are as in Fig. 1.

discrepancy among the cross sections obtained with the various models is observed, with the smallest contribution being for the RMF and the largest one for RGF-EDAI. Furthermore, the RGF with the EDAD1 optical potential gives results which are very similar to the RPWIA calculation. The predictions of these two models, RPWIA and RGF-EDAD1, agree very well with the preliminary antineutrino NCE MiniBooNE data [97,98].

The curves displayed in Figs. 7 and 8 involve a convolution over the experimental (anti)neutrino flux. In order to better understand these results, in Fig. 9 we present the proton+neutron NCE antineutrino cross section multiplied by the antineutrino MiniBooNE flux of [96] as a function of the antineutrino energy for four different values of the kinetic energy of the emitted nucleon. The calculations required for the analysis in Fig. 9 consider the entire energy range which is relevant for the MiniBooNE flux. It has been pointed out in [32,99] that the flux-average procedure introduces additional uncertainties and, therefore, the MiniBooNE cross sections can include contributions from different kinematic regions, where reaction mechanisms other than one-nucleon knockout can be dominant. Part of these contributions, which are not included in usual calculations based on the IA, can be recovered in the RGF by the imaginary part of the phenomenological OP. The RMF gives cross sections that are lower than the RPWIA ones at $T_N = 108$ and 252 MeV but larger at higher values of T_N. As already mentioned, this effect is due to the strong energy-independent potential adopted in the RMF model. The larger cross section in the RGF can be ascribed to the contribution of reaction channels which are not included in other models based on the IA.

The MiniBooNE Collaboration has also reported the $(\nu p \to \nu p)/(\nu N \to \nu N)$ ratio [18]. The denominator of this

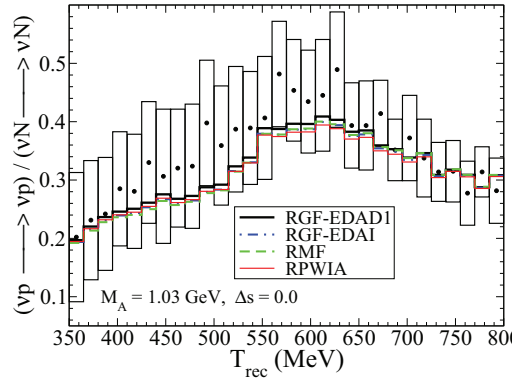

FIG. 10. (Color online) Ratio $(\nu p \to \nu p)/(\nu N \to \nu N)$ as a function of the reconstructed energy computed within RGF, RMF, and RPWIA models. Line conventions are as in Fig. 1. The data are from [18].

ratio includes events with standard NCE selection cuts but with the energy cut replaced with $350 < T_N < 800$ MeV and an additional "proton/muon" cut in order to reduce muonlike backgrounds that dominate the high-visible-energy region. In the numerator are events from the so-called NCE proton-enriched event sample where two additional cuts are applied to suppress neutron NCE events. The Monte Carlo simulation shows that only 10% of neutron NCE events give a contribution to the $\nu p \to \nu p$ sample. More details on the folding procedure to calculate this ratio are given in Appendix B of [100].

In Fig. 10 we present our results for the $(\nu p \to \nu p)/(\nu N \to \nu N)$ ratio with RGF, RMF, and RPWIA models as a function of reconstructed energy T_{rec}. In our calculations the axial strangeness Δs has been fixed to 0. All the models give very close results which are in agreement with experimental data within error bars; this is in accordance with the fact that in this kinematical regime with $T_N > 350$ MeV all the models are able to reproduce the cross-section data.

IV. CONCLUSIONS

This work extends previous comparative studies to include the analysis of neutral-current neutrino-nucleus scattering reactions. In previous works we applied our models to inclusive electron and charged-current neutrino scattering, providing also a comparison with data measured by the MiniBooNE collaboration. Our main objective in this paper is to examine how capable our theoretical models are at explaining the recent data on NC reactions measured by MiniBooNE. In both cases, CC and NC processes, the kinematics involved implies the use of fully relativistic models. This is the case of the relativistic mean-field and the relativistic Green's function approaches considered in this work. Not only is relativistic kinematics considered, but also nuclear dynamics and current operators are described within a relativistic formalism. Moreover, final state interactions, an essential ingredient in the reaction mechanism, are also taken into account by introducing relativistic potentials in the final state and solving the Dirac equation. Whereas in the RMF case the potential consists of real strong energy-independent scalar and vector terms

(the same used for the bound nucleon states), the RGF makes use of phenomenological energy-dependent complex optical potentials. In this work results are shown for two choices of the optical potential: EDAI and EDAD1.

We have compared the predictions for the differential cross sections and the proton/neutron ratio. The former shows an important dependence with the model, particularly at small values of the outgoing nucleon kinetic energy. The RMF provides the lowest result while the RGF gets much more strength, although a significant dependence on the potentials considered is also seen for the RGF case. This general result applies to both neutrino and antineutrino reactions and occurs for very different values of the lepton ($\nu_\mu/\overline{\nu}_\mu$) energy. This explains the significant differences observed for the NC flux-averaged cross sections, which are also compared with MiniBooNE data. From our analysis we conclude that the largest contribution corresponding to RGF-EDAI is in accordance with data for neutrinos, whereas the other models, in particular the RMF, lie clearly below data at small nucleon kinetic energies (T_N). In contrast, all models reproduce the behavior of data at larger T_N values. However, we have to keep in mind the large data error bands in this kinematical regime.

In addition to the uncertainties associated with nuclear model and/or FSI descriptions, which are particularly relevant for the cross sections, another ingredient to be carefully considered is the role of strangeness in the nucleon. While strangeness in the electric and magnetic sectors leads to very minor effects, which are almost negligible for the total cross section, the dependence upon the axial-vector strangeness is much more important. This is particularly true in the case of the separate proton and neutron contributions to the cross sections. The role of the axial strangeness is opposite in protons and neutrons, and it tends to cancel in the total cross section. This justifies the use of total cross sections to analyze nuclear models and FSI dependencies, since they are almost independent of Δs (axial strangeness). Moreover, it also justifies the use of the p/n ratio as a useful observable to get information on the axial strangeness.

In this work we have analyzed in detail the proton/neutron ratio by comparing the predictions given by the RMF and RGF models. We have proved that the ratio only presents a weak dependence on the model, in particular, in the case of neutrinos: the uncertainty is on average of the order of $\sim 4\%$–5%. This discrepancy gets significantly higher for antineutrinos at increasing values of nucleon energy. In any case, these differences are usually smaller than the ones ascribed to the use of different axial strangeness content in the nucleon. In this case the p/n ratio can change by more than a factor of 2 when the variation in Δs is in accordance with the Brookhaven and MiniBooNE data. However, the highly precise measurements given by COMPASS lead to an uncertainty in $R[p/n]$ similar to the one ascribed to distortion and nuclear model effects.

Summarizing, we have applied two different relativistic models that incorporate final-state interactions to the study of NCE neutrino- and antineutrino-nucleus scattering processes. We have presented a detailed analysis of the differential cross sections (with the separate proton and neutron contributions) and the p/n ratio. We have compared our predictions with the recent experimental data taken by the MiniBooNE Collaboration for neutrinos and have given predictions for antineutrinos which can be also compared with data when available. We have proved the significant differences introduced by the various models that may indicate important effects ascribed to correlation and meson exchange currents, which are not yet incorporated in the models. Although the comparison between RMF and RGF models may help us in disentangling different aspects involved in the physics of the problem, we should be cautious in establishing final conclusions before other ingredients beyond the impulse approximation can be implemented in more refined calculations and their contributions can be carefully examined.

ACKNOWLEDGMENTS

This work was partially supported by the Italian MIUR through the PRIN 2009 research project, by the Istituto Nazionale di Fisica Nucleare under Contract No. MB31, by Spanish DGI and FEDER funds (FIS2011-28738-C02-01 and FPA2010-17142), by the Junta de Andalucia, by the Spanish Consolider-Ingenio 2000 program CPAN (CSD2007-00042), by the Campus of Excellence International (CEI) of the Moncloa project (Madrid) and Andalucia Tech, by the INFN-MICINN collaboration agreement (AIC-D-2011-0704), as well as by the Bulgarian National Science Fund under Contracts No. DO-02-285 and No. DID-02/16-17.12.2009. MVI is grateful for the warm hospitality given by the UCM and for financial support during his stay there from the SiNuRSE action within the ENSAR European project. RGJ acknowledges support from the Ministerio de Educación (Spain).

[1] K. Abe *et al.* (Super-Kamiokande Collaboration), Phys. Rev. D **83**, 052010 (2011).
[2] K. Abe *et al.* (Super-Kamiokande Collaboration), Phys. Rev. Lett. **107**, 241801 (2011).
[3] M. Antonello *et al.* (ICARUS Collaboration), Eur. Phys. J. C **73**, 1 (2013).
[4] B. Aharmim *et al.* (SNO Collaboration), Phys. Rev. C **81**, 055504 (2010).
[5] P. Adamson *et al.* (MINOS Collaboration), Phys. Rev. Lett. **107**, 021801 (2011).
[6] K. Abe *et al.* (T2K Collaboration), Phys. Rev. Lett. **107**, 041801 (2011).
[7] A. A. Aguilar-Arevalo *et al.* (MiniBooNE Collaboration), Phys. Rev. Lett. **110**, 161801 (2013).
[8] K. B. M. Mahn *et al.* (MiniBooNE and SciBooNE Collaborations), Phys. Rev. D **85**, 032007 (2012).

[9] G. Cheng *et al*. (MiniBooNE and SciBooNE Collaborations), Phys. Rev. D **86**, 052009 (2012).
[10] Y. Abe *et al*. (Double Chooz Collaboration), Phys. Rev. Lett. **108**, 131801 (2012).
[11] F. P. An *et al*. (Daya Bay Collaboration), Phys. Rev. Lett. **108**, 171803 (2012).
[12] F. P. An *et al*. (Daya Bay Collaboration), Chin. Phys. C **37**, 011001 (2013).
[13] J. K. Ahn *et al*. (RENO Collaboration), Phys. Rev. Lett. **108**, 191802 (2012).
[14] M. H. Ahn *et al*. (K2K Collaboration), Phys. Rev. D **74**, 072003 (2006).
[15] A. Aguilar *et al*. (LSND Collaboration), Phys. Rev. D **64**, 112007 (2001).
[16] L. A. Ahrens *et al*., Phys. Rev. D **35**, 785 (1987).
[17] A. A. Aguilar-Arevalo *et al*. (MiniBooNE Collaboration), Phys. Rev. D **81**, 092005 (2010).
[18] A. A. Aguilar-Arevalo *et al*. (MiniBooNE Collaboration), Phys. Rev. D **82**, 092005 (2010).
[19] A. A. Aguilar-Arevalo *et al*. (MiniBooNE Collaboration), Phys. Rev. D **88**, 032001 (2013).
[20] Y. Nakajima *et al*. (SciBooNE Collaboration), Phys. Rev. D **83**, 012005 (2011).
[21] C. Anderson *et al*. (ArgoNeuT Collaboration), Phys. Rev. Lett. **108**, 161802 (2012).
[22] http://www-boone.fnal.gov
[23] http://minerva.fnal.gov/
[24] http://t2k-experiment.org/
[25] V. Bernard, L. Elouadrhiri, and U. G. Meissner, J. Phys. G **28**, R1 (2002).
[26] A. Bodek, S. Avvakumov, R. Bradford, and H. Budd, Eur. Phys. J. C **53**, 349 (2008).
[27] J. E. Amaro, M. B. Barbaro, J. A. Caballero, T. W. Donnelly, A. Molinari, and I. Sick, Phys. Rev. C **71**, 015501 (2005).
[28] S. Boffi, C. Giusti, and F. D. Pacati, Phys. Rep. **226**, 1 (1993).
[29] S. Boffi, C. Giusti, F. D. Pacati, and M. Radici, *Electromagnetic Response of Atomic Nuclei*, Oxford Studies in Nuclear Physics Vol. 20 (Clarendon, Oxford, 1996).
[30] J. E. Amaro, M. B. Barbaro, J. A. Caballero, and T. W. Donnelly, Phys. Rev. C **73**, 035503 (2006).
[31] A. N. Antonov, M. V. Ivanov, M. B. Barbaro, J. A. Caballero, E. Moya de Guerra, and M. K. Gaidarov, Phys. Rev. C **75**, 064617 (2007).
[32] O. Benhar and G. Veneziano, Phys. Lett. B **702**, 433 (2011).
[33] A. M. Ankowski, Phys. Rev. C **86**, 024616 (2012).
[34] M. Martini, M. Ericson, G. Chanfray, and J. Marteau, Phys. Rev. C **80**, 065501 (2009).
[35] M. Martini, M. Ericson, G. Chanfray, and J. Marteau, Phys. Rev. C **81**, 045502 (2010).
[36] M. Martini, M. Ericson, and G. Chanfray, Phys. Rev. C **84**, 055502 (2011).
[37] M. Martini and M. Ericson, Phys. Rev. C **87**, 065501 (2013).
[38] J. Nieves, I. Ruiz Simo, and M. J. Vicente Vacas, Phys. Rev. C **83**, 045501 (2011).
[39] J. Nieves, I. Ruiz Simo, and M. J. Vicente Vacas, Phys. Lett. B **707**, 72 (2012).
[40] J. Nieves, I. Ruiz Simo, and M. J. Vicente Vacas, Phys. Lett. B **721**, 90 (2013).
[41] A. De Pace, M. Nardi, W. M. Alberico, T. W. Donnelly, and A. Molinari, Nucl. Phys. A **741**, 249 (2004).
[42] J. E. Amaro, M. B. Barbaro, J. A. Caballero, T. W. Donnelly, and C. F. Williamson, Phys. Lett. B **696**, 151 (2011).
[43] J. E. Amaro, M. B. Barbaro, J. A. Caballero, T. W. Donnelly, and J. M. Udías, Phys. Rev. D **84**, 033004 (2011).
[44] J. E. Amaro, M. B. Barbaro, J. A. Caballero, and T. W. Donnelly, Phys. Rev. Lett. **108**, 152501 (2012).
[45] A. Bodek, H. Budd, and M. Christy, Eur. Phys. J. C **71**, 1 (2011).
[46] T. Golan, K. M. Graczyk, C. Juszczak, and J. T. Sobczyk, arXiv:1302.3890 [hep-ph].
[47] T. Leitner, O. Buss, L. Alvarez-Ruso, and U. Mosel, Phys. Rev. C **79**, 034601 (2009).
[48] T. Leitner and U. Mosel, Phys. Rev. C **81**, 064614 (2010).
[49] A. M. Ankowski and O. Benhar, Phys. Rev. C **83**, 054616 (2011).
[50] E. Fernandez Martinez and D. Meloni, Phys. Lett. B **697**, 477 (2011).
[51] J. G. Morfin, J. Nieves, and J. T. Sobczyk, Adv. High Energy Phys. **2012**, 934597 (2012).
[52] J. M. Udías, P. Sarriguren, E. Moya de Guerra, E. Garrido, and J. A. Caballero, Phys. Rev. C **48**, 2731 (1993).
[53] A. Meucci, C. Giusti, and F. D. Pacati, Phys. Rev. C **64**, 014604 (2001).
[54] A. Meucci, C. Giusti, and F. D. Pacati, Phys. Rev. C **64**, 064615 (2001).
[55] A. Meucci, Phys. Rev. C **65**, 044601 (2002).
[56] M. Radici, A. Meucci, and W. H. Dickhoff, Eur. Phys. J. A **17**, 65 (2003).
[57] C. Giusti, A. Meucci, F. D. Pacati, G. Co', and V. De Donno, Phys. Rev. C **84**, 024615 (2011).
[58] C. Maieron, M. C. Martinez, J. A. Caballero, and J. M. Udías, Phys. Rev. C **68**, 048501 (2003).
[59] J. A. Caballero, Phys. Rev. C **74**, 015502 (2006).
[60] J. A. Caballero, M. C. Martinez, J. L. Herraiz, and J. M. Udías, Phys. Lett. B **688**, 250 (2010).
[61] A. Meucci, C. Giusti, and F. D. Pacati, Nucl. Phys. A **739**, 277 (2004).
[62] A. Meucci, F. Capuzzi, C. Giusti, and F. D. Pacati, Phys. Rev. C **67**, 054601 (2003).
[63] A. Meucci, C. Giusti, and F. D. Pacati, Nucl. Phys. A **744**, 307 (2004).
[64] A. Meucci, C. Giusti, and F. D. Pacati, Acta Phys. Pol. B **37**, 2279 (2006).
[65] A. Meucci, C. Giusti, and F. D. Pacati, Nucl. Phys. A **773**, 250 (2006).
[66] A. Meucci, C. Giusti, and F. D. Pacati, Phys. Rev. C **77**, 034606 (2008).
[67] C. Giusti, A. Meucci, and F. D. Pacati, Acta Phys. Pol. B **40**, 2579 (2009).
[68] A. Meucci, J. A. Caballero, C. Giusti, F. D. Pacati, and J. M. Udías, Phys. Rev. C **80**, 024605 (2009).
[69] A. Meucci, J. A. Caballero, C. Giusti, and J. M. Udías, Phys. Rev. C **83**, 064614 (2011).
[70] C. Giusti and A. Meucci, EPJ Web Conf. **38**, 14004 (2012).
[71] J. A. Caballero, J. E. Amaro, M. B. Barbaro, T. W. Donnelly, C. Maieron, and J. M. Udías, Phys. Rev. Lett. **95**, 252502 (2005).
[72] Y. Horikawa, F. Lenz, and N. C. Mukhopadhyay, Phys. Rev. C **22**, 1680 (1980).
[73] F. Capuzzi, C. Giusti, and F. D. Pacati, Nucl. Phys. A **524**, 681 (1991).

[74] F. Capuzzi, C. Giusti, F. D. Pacati, and D. N. Kadrev, Ann. Phys. (NY) **317**, 492 (2005).
[75] A. Meucci, C. Giusti, and F. D. Pacati, Nucl. Phys. A **756**, 359 (2005).
[76] C. Giusti and A. Meucci, J. Phys.: Conf. Ser. **336**, 012025 (2011).
[77] A. Meucci, M. Vorabbi, C. Giusti, F. D. Pacati, and P. Finelli, Phys. Rev. C **87**, 054620 (2013).
[78] A. Meucci, C. Giusti, and M. Vorabbi, Phys. Rev. D **88**, 013006 (2013).
[79] A. Meucci, M. B. Barbaro, J. A. Caballero, C. Giusti, and J. M. Udías, Phys. Rev. Lett. **107**, 172501 (2011).
[80] A. Meucci, C. Giusti, and F. D. Pacati, Phys. Rev. D **84**, 113003 (2011).
[81] B. D. Serot and J. D. Walecka, Adv. Nucl. Phys. **16**, 1 (1986).
[82] E. D. Cooper, S. Hama, B. C. Clark, and R. L. Mercer, Phys. Rev. C **47**, 297 (1993).
[83] A. Meucci and C. Giusti, Phys. Rev. D **85**, 093002 (2012).
[84] R. González-Jiménez, J. A. Caballero, and T. W. Donnelly, Phys. Rep. **524**, 1 (2013).
[85] G. T. Garvey, W. C. Louis, and D. H. White, Phys. Rev. C **48**, 761 (1993).
[86] R. González-Jiménez, M. V. Ivanov, M. B. Barbaro, J. A. Caballero, and J. M. Udías, Phys. Lett. B **718**, 1471 (2013).
[87] V. Y. Alexakhin *et al*. (COMPASS Collaboration), Phys. Lett. B **647**, 8 (2007).
[88] A. Airapetian *et al*. (HERMES Collaboration), Phys. Rev. D **75**, 012007 (2007).
[89] G. Garvey, E. Kolbe, K. Langanke, and S. Krewald, Phys. Rev. C **48**, 1919 (1993).
[90] M. B. Barbaro, A. De Pace, T. W. Donnelly, A. Molinari, and M. J. Musolf, Phys. Rev. C **54**, 1954 (1996).
[91] W. M. Alberico *et al*., Phys. Lett. B **438**, 9 (1998).
[92] W. M. Alberico, S. M. Bilenky, and C. Maieron, Phys. Rep. **358**, 227 (2002).
[93] P. Lava, N. Jachowicz, M. C. Martinez, and J. Ryckebusch, Phys. Rev. C **73**, 064605 (2006).
[94] C. Praet, N. Jachowicz, J. Ryckebusch, P. Vancraeyveld, and K. Vantournhout, Phys. Rev. C **74**, 065501 (2006).
[95] N. Jachowicz, P. Vancraeyveld, P. Lava, C. Praet, and J. Ryckebusch, Phys. Rev. C **76**, 055501 (2007).
[96] A. A. Aguilar-Arevalo *et al*. (MiniBooNE Collaboration), Phys. Rev. D **84**, 072005 (2011).
[97] R. Dharmapalan, Ph.D. thesis, University of Alabama, 2012.
[98] J. Grange and R. Dharmapalan (MiniBooNE Collaboration), arXiv:1304.7395 [hep-ph].
[99] O. Benhar, P. Coletti, and D. Meloni, Phys. Rev. Lett. **105**, 132301 (2010).
[100] D. Perevalov, Ph.D. thesis, University of Alabama, 2009.